Journal of Organometallic Chemistry, 320 (1987) 257–266
Elsevier Sequoia S.A., Lausanne – Printed in The Netherlands

THE SYNTHESIS AND STRUCTURAL CHARACTERISATION OF $[Pt_3Au_2(\mu\text{-}Cl)(\mu\text{-}SO_2)_2(PCy_3)_3(P\{p\text{-}C_6H_4F\}_3)_2](PF_6)$: THE FIRST EXAMPLE OF A TRIGONAL-BIPYRAMIDAL PLATINUM–GOLD CLUSTER COMPOUND

D. MICHAEL P. MINGOS *, PAUL OSTER and DARREN J. SHERMAN

Inorganic Chemistry Laboratory, University of Oxford, South Parks Road, Oxford OX1 3QR (Great Britain)

(Received August 8th, 1986)

Summary

$[Pt_3Au_2(\mu\text{-}Cl)(\mu\text{-}SO_2)_2(PCy_3)_3(P\{p\text{-}C_6H_4F\}_3)_2](PF_6)$ has been synthesised from $[Pt_3Au(\mu\text{-}Cl)(\mu\text{-}SO_2)_2(PCy_3)_3(P\{p\text{-}C_6H_4F\}_3)]$ and $[AuCl(P\{p\text{-}C_6H_4F\}_3)]$ in the presence of $TlPF_6$. The compound has been characterised as a trigonal-bipyramidal cluster, with gold atoms occupying the apical sites, on the basis of $^{31}P\{^1H\}$ and $^{195}Pt\{^1H\}$ NMR spectroscopy and a single crystal X-ray crystallographic analysis.

Introduction

Until recently no examples of platinum–gold cluster compounds had been structurally characterised, although a large number of heteronuclear clusters of other Group VIII metals and gold are known, thus raising doubts about the stability of cluster compounds containing Pt–Au bonds. Mingos and Wardle, in a study of the chemistry of the *triangulo*-triplatinum clusters $[Pt_3(\mu\text{-}X)_3(PCy_3)_3]$ (X = CO or SO_2), demonstrated that they are sufficiently nucleophilic to react with $[AuCl(PCy_3)]$, in the presence of $TlPF_6$, to give the 54-electron tetrahedral clusters $[Pt_3Au(\mu\text{-}X)_3(PCy_3)_4](PF_6)$ in high yield [1,2]. In addition, the sulphur-dioxide cluster was found to react readily with $[AuCl(P\{p\text{-}C_6H_4F\}_3)]$ in the absence of $TlPF_6$, to give the 56-electron tetrahedral cluster $[Pt_3Au(\mu\text{-}Cl)(\mu\text{-}SO_2)_2(PCy_3)_3(P\{p\text{-}C_6H_4F\}_3)]$ (**1**) [2]. Subsequently Mingos and Gilmour have reported the synthesis and structure of the 56-electron tetranuclear cluster $[Pt_2Au_2(CNC_8H_9)_4(PPh_3)_4](PF_6)_2$, which has a butterfly geometry [3], and Braunstein and co-workers have synthesised the *triangulo*-cluster $[Pt(AuPPh_3)_2Cl(PEt_3)_2](CF_3SO_3)$ [4].

Mingos and Wardle [5] found that no further reaction occurred between the 54-electron cluster $[Pt_3Au(\mu\text{-}CO)_3(PCy_3)_4]^+$ and $[AuCl(PCy_3)]$ even in the presence of $TlPF_6$. The 56-electron cluster $[Pt_3Au(\mu\text{-}Cl)(\mu\text{-}SO_2)_2(PCy_3)_3(P\{p\text{-}C_6H_4F\}_3)]$ (**1**) is neutral and has an extra electron pair occupying the relatively high lying a_2 HOMO [6] which should render the cluster more nucleophilic. This paper describes the reaction of this cluster with $[Au(PR_3)]^+$.

0022-328X/87/$03.50

Results and discussion

When a benzene solution of **1** was added to [AuCl(P{ *p*-C_6H_4F}$_3$)] no reaction was observed, but on stirring with excess $TlPF_6$ an orange-brown solid separated. Recrystallisation of this powder from dichloromethane/hexane gave an orange-yellow microcrystalline solid which analysed satisfactorily for [Pt_3Au_2(μ-Cl)(μ-SO_2)$_2$(PCy_3)$_3$(P{ *p*-C_6H_4F}$_3$)$_2$](PF_6) (**2**) in 74% yield.

The infra-red spectrum of **2** [$\nu(SO_2)$ (cm^{-1}) 1058s and 1162s] is very similar to that reported for **1**. The $^{31}P\{^1H\}$ and $^{195}Pt\{^1H\}$ NMR spectra are, however, distinctly different and confirm the retention of the unsymmetrically bridged *triangulo*-triplatinum unit. The $^{31}P\{^1H\}$ spectrum is shown in Fig. 1. It shows resonances at δ 37.1 [m, 2P, $PtPCy_3$], 23.6 [m, 2P, AuP(*p*-C_6H_4F)$_3$] and 21.4 [m, 1P, $PtPCy_3$] ppm relative to TMP. The important difference between this spectrum and that of **1** is the loss of P_{Pt}–P_{Au} coupling in the former, though the ^2J(Pt–P_{Au}) coupling is still observable. The spectrum has been satisfactorily simulated using a computer analysis based on the following isotopomers: A_2B_2C (no ^{195}Pt), $AA'B_2CX$ and A_2B_2CY (one ^{195}Pt nucleus), $AA'B_2CXX'$ and $AA'B_2CXY$ (two ^{195}Pt nuclei) [7].

The $^{195}Pt\{^1H\}$ NMR spectrum, shown in Fig. 2, consists of two resonances at −3908.7 and −5245.1 ppm with respect to Na_2PtCl_6 in the ratio 2/1. The coupling constants derived from the computer simulations of both the $^{31}P\{^1H\}$ and

(*Continued on p. 261*)

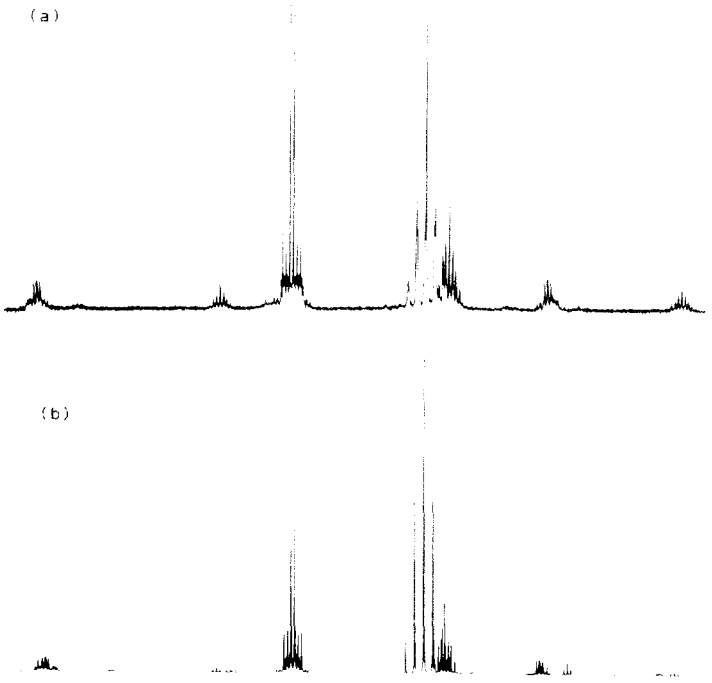

Fig. 1. (a) Observed and (b) calculated $^{31}P\{^1H\}$ NMR spectra for [Pt_3Au_2(μ-Cl)(μ-SO_2)$_2$(PCy_3)$_3$(P{ *p*-C_6H_4F}$_3$)$_2$]PF_6 (**2**).

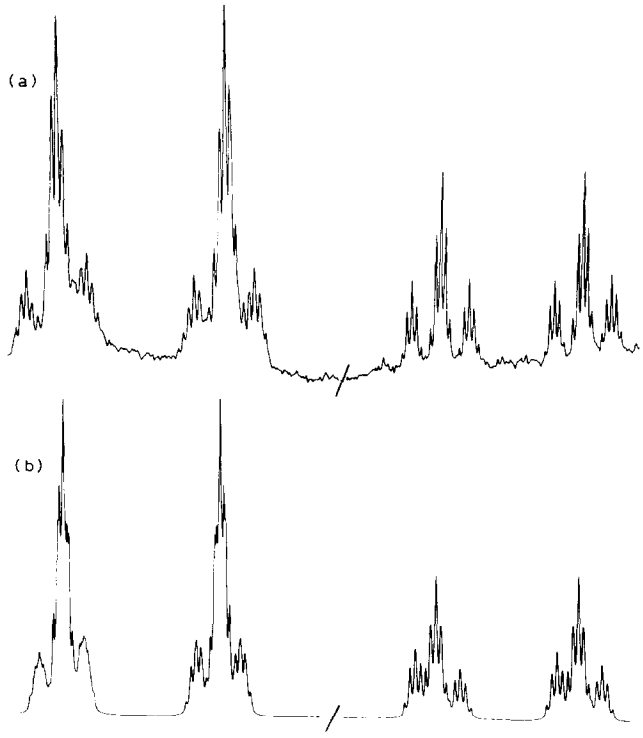

Fig. 2. (a) Observed and (b) calculated $^{195}Pt\{^{1}H\}$ NMR spectra for $[Pt_3Au_2(\mu\text{-}Cl)(\mu\text{-}SO_2)_2(PCy_3)_3(P\{p\text{-}C_6H_4F\}_3)_2]PF_6$ (**2**).

TABLE 1

OBSERVED CHEMICAL SHIFTS AND COUPLING CONSTANTS FOR THE COMPLEX $[Pt_3Au_2(\mu\text{-}Cl)(\mu\text{-}SO_2)_2(PCy_3)_3(P\{p\text{-}C_6H_4F\}_3)_2](PF_6)$ (**2**) DERIVED FROM THE $^{31}P\{^{1}H\}$ AND $^{195}Pt\{^{1}H\}$ NMR SPECTRA

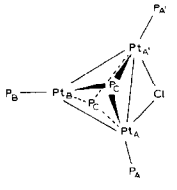

	P_A	P_B	P_C		Pt_A	Pt_B
δ (ppm)	37.1	21.4	23.6		−3908.7	−5245.1
J (Hz)	Pt_A	$Pt_{A'}$	Pt_B	P_A	$P_{A'}$	P_B
P_C	190.0	190.0	190.0	0.0	0.0	0.0
P_B	132.5	132.5	4640.0	37.2	37.2	
$P_{A'}$	121.0	5158.0	147.9	26.9		
Pt_B	[a]	[a]				
$Pt_{A'}$	[a]					

[a] The value of the Pt–Pt coupling constant was not measurable from the experimental observations.

TABLE 2. CRYSTAL DATA FOR $[Pt_3Au_2(\mu\text{-}Cl)(\mu\text{-}SO_2)_2(PCy_3)_3(P\{p\text{-}C_6H_4F\}_3)_2][PF_6]$ (**2**) AND DETAILS OF DATA COLLECTION AND STRUCTURE ANALYSIS

Formula $C_{90}H_{123}Au_2ClF_{12}O_4P_7Pt_3S_2$	$[Pt_3Au_2Cl(SO_2)_2(P\{C_6H_{11}\}_3)_3(P\{p\text{-}C_6H_4F\}_3)_2][PF_6]$
Formula weight	2761.29
Space group	$P\bar{1}$
a (Å)	14.224(8)
b (Å)	14.432(5)
c (Å)	29.424(11)
α (°)	97.04(3)
β (°)	94.44(4)
γ (°)	111.51(4)
V (Å^3)	5527.45
Z	2
D_c (g cm^{-3})	1.66
Radiation Mo-K_α	λ 0.71069 Å, graphite monochromator
Temperature	294 K
μ	64.5 cm^{-1}
Scan mode	$\omega/2\theta$, $1.0° < \theta < 22.5°$ ($h, +k, \pm l$)
Scan width (°)	$0.90 + 0.35\tan\theta$
Total data collected	17524 reflections
Total unique data ($I \geqslant 3\sigma(I)$)	8267
Merging R-value	0.0560
$R = \Sigma\|\|F_o\| - \|F_c\|\|/\Sigma F_o$	0.0709
$R_w = [\Sigma w(\|F_o\| - \|F_c\|)^2/\Sigma wF_o^2]^{1/2}$	0.0934
Weighting scheme Chebyshev coefficients	161.98 217.92 and 69.76

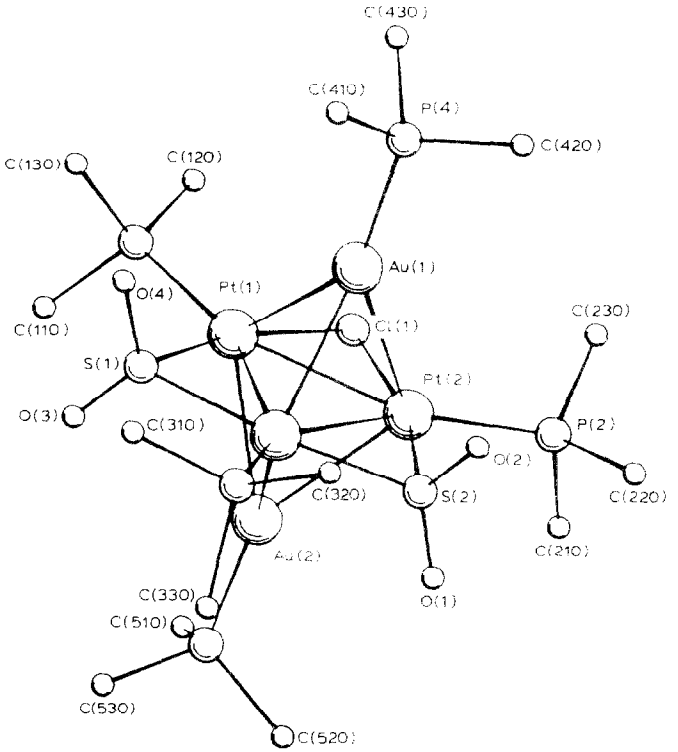

Fig. 3. The molecular geometry of the cation in $[Pt_3Au_2(\mu\text{-}Cl)(\mu\text{-}SO_2)_2(PCy_3)_3(P\{p\text{-}C_6H_4F\}_3)_2][PF_6]$ (**2**). For reasons of clarity only one of the carbon atoms of each Ph and cyclohexyl ring is shown. In the structure the SO_2 and Cl bridging ligands are disordered.

TABLE 3

SELECTED MOLECULAR DIMENSIONS FOR $[Pt_3Au_2(\mu\text{-}Cl)(\mu\text{-}SO_2)(PCy_3)_3(P\{p\text{-}C_6H_4F\}_3)_2](PF_6)$ (**2**) (with estimated standard deviations in parentheses)

Intramolecular dimensions (Å)		*Bond angles (°)*	
Pt(1)–Pt(2)	2.887(2)	Pt(3)–Pt(1)–Pt(2)	59.92(4)
Pt(1)–Pt(3)	2.888(2)	Au(1)–Pt(1)–Pt(2)	58.36(5)
Pt(1)–Au(1)	2.803(2)	Au(1)–Pt(1)–Pt(3)	58.95(4)
Pt(1)–Au(2)	2.776(2)	Au(2)–Pt(1)–Pt(2)	58.59(4)
Pt(2)–Pt(3)	2.884(2)	Au(2)–Pt(1)–Pt(3)	58.83(4)
Pt(2)–Au(1)	2.775(2)	Au(2)–Pt(1)–Au(1)	106.27(6)
Pt(2)–Au(2)	2.772(2)	Pt(3)–Pt(2)–Pt(1)	60.07(4)
Pt(3)–Au(1)	2.801(2)	Au(1)–Pt(2)–Pt(1)	59.32(5)
Pt(3)–Au(2)	2.784(2)	Au(1)–Pt(2)–Pt(3)	59.31(5)
Pt(1)–P(1)	2.311(8)	Au(2)–Pt(2)–Pt(1)	58.70(4)
Pt(1)–Cl(1)	2.319(8)	Au(2)–Pt(2)–Pt(3)	58.92(4)
Pt(1)–S(1)	2.311(8)	Au(2)–Pt(2)–Au(1)	107.14(6)
Pt(2)–P(2)	2.305(8)	Pt(2)–Pt(3)–Pt(1)	60.01(4)
Pt(2)–Cl(1)	2.344(8)	Au(1)–Pt(3)–Pt(1)	59.01(4)
Pt(2)–S(2)	2.321(9)	Au(1)–Pt(3)–Pt(2)	58.42(5)
Pt(3)–P(3)	2.320(7)	Au(2)–Pt(3)–Pt(1)	58.57(4)
Pt(3)–S(1)	2.329(8)	Au(2)–Pt(3)–Pt(2)	58.54(4)
Pt(3)–S(2)	2.325(8)	Au(2)–Pt(3)–Au(1)	106.11(5)
Au(1)–P(4)	2.243(9)	Pt(2)–Au(1)–Pt(1)	62.32(5)
Au(2)–P(5)	2.249(9)	Pt(3)–Au(1)–Pt(1)	62.04(4)
S(1)–O(3)	1.23(3)	Pt(3)–Au(1)–Pt(2)	62.28(5)
S(1)–O(4)	1.53(3)	Pt(3)–Au(2)–Pt(1)	62.60(4)
S(2)–O(1)	1.27(3)	Pt(3)–Au(2)–Pt(1)	62.60(4)
S(2)–O(2)	1.49(3)	Pt(3)–Au(2)–Pt(2)	62.54(4)
		S(1)–Pt(1)–Cl(1)	163.7(3)
		P(1)–Pt(1)–Cl(1)	97.9(3)
		P(1)–Pt(1)–S(1)	98.4(3)
		S(2)–Pt(2)–Cl(1)	163.1(3)
		P(2)–Pt(2)–Cl(1)	98.6(3)
		P(2)–Pt(2)–S(2)	98.6(3)
		S(1)–Pt(3)–S(2)	162.6(3)
		P(3)–Pt(3)–S(1)	99.1(3)
		P(3)–Pt(3)–S(2)	98.3(3)
		Pt(1)–S(1)–Pt(3)	77.0(2)
		Pt(2)–S(2)–Pt(3)	76.7(3)
		Pt(1)–Cl(1)–Pt(2)	76.5(2)
		O(3)–S(1)–O(4)	119.3(20)
		O(1)–S(2)–O(2)	118.9(18)

$^{195}Pt\{^1H\}$ NMR spectra are given in Table 1. In order to fully characterise this novel platinum-gold cluster, and confirm its trigonal-bipyramidal geometry, a single crystal X-ray crystallographic analysis was undertaken.

The relevant details of the crystallographic study are given in Table 2. Selected intramolecular bond lengths and angles are given in Table 3 and fractional coordinates for the non-hydrogen atoms in Table 4. The structure of the molecule is illustrated in Fig. 3.

Discussion of the crystal structure

As indicated by the spectroscopic analysis detailed above, the cation consists of five metal atoms defining a slightly distorted trigonal-bipyramid. The Pt–Pt–Pt, Pt–Pt–Au and Pt–Au–Pt angles are all close to their idealised value of 60°, though the polyhedron is squashed slightly in the axial direction, because the Pt–Au bonds are slightly shorter than the Pt–Pt bonds.

The bridging ligands remain coordinated exclusively to the platinum atoms, and the bond lengths to them fall in the usual range. The tricyclohexylphosphine ligands and the bridging groups are essentially coplanar with the Pt_3 triangle.

The metal–metal distances in **2** are contrasted with those of related clusters based on *triangulo*-triplatinum units in Table 5 and illustrate the increased Pt–Pt distances in the clusters based on 44-electron triangles compared with those based on 42-electrons. In addition, capping of a triangle with an $[Au(PR_3)]^+$ fragment leads to a lengthening of these bonds.

Calculations on model clusters [6] have yielded Mulliken overlap populations for the Pt–Pt and Pt–Au bonds (Table 6) which reproduce the trends in bond lengths noted above, and are interpretable in terms of the population of an orbital of a_2' symmetry, similar to that illustrated in **3**.

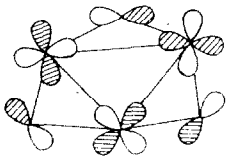

a_2' (**3**)

The introduction of the bridging chloride ligand stabilises the a_2' orbital of the triangular, tetrahedral and trigonal-bipyramidal clusters, and occupation of this orbital, which is slightly metal–metal antibonding, leads to a weakening of the platinum–platinum bonds. Since the $[Au(PR_3)]$ fragment does not have any frontier orbitals of a_2 symmetry, the occupation of this orbital has little effect on the Pt–Au bonding, and the Pt–Au bond lengths are essentially unaffected by the electron count.

The Pt–Au bonding in the cluster **2** is best described in terms of a five-centre two-electron bond. The interaction of the a_1 orbital of the Pt_3Au tetrahedron with the $[Au(PR_3)]$ fragment leads to reduced Pt–Pt bonding character in the resulting molecular orbital, and consequently lower overlap population and longer bonds than in **1**. This analysis is consistent with the presence of 68 valence electrons in **2**.

Since in both $[Pt_3(\mu\text{-}SO_2)_3(PCy_3)_3]$ [8] and $[Pt_3Au(\mu\text{-}SO_2)_3(PCy_3)_4]^+$ [2] the sulphur dioxide ligands can be substituted by chloride, the reaction of $[Me_4N]Cl$ with $[Pt_3Au_2(\mu\text{-}Cl)(\mu\text{-}SO_2)_2(PCy_3)_3(P\{p\text{-}C_6H_4F\}_3)_2](PF_6)$ (**2**) was studied. It was possible that the complex $[Pt_3Au_2(\mu\text{-}Cl)_2(\mu\text{-}SO_2)(PCy_3)_3(P\{p\text{-}C_6H_4F\}_3)_2]$ would result, which would be a derivative of the 46-electron triangle $[Pt_3(\mu\text{-}Cl)_2(\mu\text{-}SO_2)(PCy_3)_3]^{2-}$. *Triangulo*-triplatinum clusters with high electron counts are stabilised by the presence of capping ligands, e.g. the 48-electron complex $[Pt_3(\mu_3\text{-}S)_2(PMePh_2)_6]^{2+}$ [9]. Reaction of $[Me_4N]Cl$ with **2** in dichloromethane led to a slow colour change from dark to light orange. On evaporation of solvent and

(*Continued on p. 265*)

TABLE 4

FINAL FRACTIONAL ATOMIC COORDINATES ($\times 10^4$) AND ISOTROPIC TEMPERATURE FACTORS ($Å^2 \times 10^4$) FOR $[Pt_3Au_2(\mu\text{-}Cl)(\mu\text{-}SO_2)_2(PCy_3)_3(P\{p\text{-}C_6H_4F\}_2)_2](PF_6)$ (**2**) (with estimated standard deviations in parentheses)

Atom	x	y	z	U_{iso}
Pt(1)	569.1(8)	2523.2(8)	7212.2(4)	342
Pt(2)	2558.4(8)	3695.5(9)	7723.5(5)	360
Pt(3)	1049.4(9)	4583.0(8)	7640.0(5)	345
Au(1)	1980(1)	4145(1)	6882.0(5)	566
Au(2)	833(1)	3058(1)	8165.9(5)	498
P(1)	−532(6)	1069(6)	6737(3)	423
P(2)	4199(6)	3848(6)	7963(3)	398
P(3)	610(6)	5983(6)	7765(3)	418
P(4)	2517(6)	4694(6)	6231(3)	440
P(5)	255(6)	2493(6)	8810(3)	420
Cl(1)	1926(6)	2020(6)	7343(4)	553
S(1)	−478(7)	3427(6)	7225(3)	465
S(2)	2693(6)	5303(6)	8037(4)	499
O(1)	2836(22)	5460(22)	8475(11)	550(80)
O(2)	3323(20)	6094(20)	7785(10)	491(74)
O(3)	−1219(26)	3104(25)	7433(12)	739(96)
O(4)	−630(22)	3696(22)	6744(11)	620(83)
O(5)	2447(27)	1966(27)	6916(13)	380(94)
O(6)	1708(27)	1239(27)	7600(13)	368(93)
C(110)	−1570(19)	242(19)	7050(8)	393(73)
C(111)	−1065(19)	20(24)	7483(10)	761(114)
C(112)	−1875(22)	−731(21)	7725(11)	689(104)
C(113)	−2634(21)	−251(22)	7875(9)	528(87)
C(114)	−3110(20)	38(28)	7455(11)	976(143)
C(115)	−2287(23)	763(21)	7206(11)	723(109
C(120	120(21)	209(19)	6538(9)	524(86)
C(121)	816(25)	616(22)	6171(12)	797(118)
C(122)	1507(25)	7(30)	6105(17)	1386(207)
C(123)	853(34)	−1124(29)	5954(15)	1357(201)
C(124)	117(30)	−1513(24)	6306(15)	1161(169)
C(125)	−577(20)	−903(20)	6353(12)	739(111)
C(130)	−1221(21)	1362(21)	6265(8)	534(87)
C(131)	−2030(25)	428(20)	5951(11)	833(123)
C(132)	−2639(23)	785(29)	5602(13)	1091(159)
C(133)	−1911(32)	1462(33)	5306(11)	1393(208)
C(134)	−1103(30)	2392(25)	5624(14)	1169(171)
C(135)	−493(20)	2045(25)	5974(12)	855(126)
C(210)	4268(20)	3271(19)	8493(9)	494(82)
C(211)	3912(26)	3805(21)	8886(10)	759(114)
C(212)	4062(28)	3357(23)	9322(10)	925(136)
C(213)	3386(27)	2222(23)	9246(11)	905(133)
C(214)	3681(27)	1669(21)	8838(11)	827(123)
C(215)	3578(26)	2138(20)	8401(10)	874(128)
C(514)	−917(14)	−422(18)	9033(5)	861(127)
C(515)	−763(13)	590(18)	9028(5)	861(126)
F(51)	−471(17)	−1819(25)	8800(6)	1579(123)
C(520)	1124(12)	3147(15)	9320(7)	425(76)
C(521)	1181(13)	2675(15)	9701(8)	628(98)
C(522)	1842(13)	3217(16)	10102(8)	928(137)
C(523)	2442(13)	4234(16)	10118(7)	778(116)
C(524)	2390(12)	4711(15)	9738(7)	669(102)

(*continued*)

TABLE 4 (continued)

Atom	x	y	z	U_{iso}
C(525)	1730(12)	4164(15)	9339(7)	608(95)
F(52)	3067(15)	4754(19)	10490(9)	1205(91)
C(530)	924(15)	2626(7)	8910(8)	513(85)
C(531)	1589(17)	2553(7)	8523(8)	720(108)
C(532)	−2524(17)	2628(8)	8581(8)	928(136)
C(533)	2781(16)	2770(8)	9024(8)	924(134)
C(534)	−2121(17)	2841(8)	9413(8)	778(116)
C(535)	1187(16)	2768(8)	9353(8)	691(105)
F(53)	3664(24)	2840(8)	9083(10)	1597(124)
P(6)	−2102(22)	421(22)	218(11)	1126
F(61)	−3159(28)	198(39)	304(22)	1490
F(62)	−1050(30)	1066(51)	131(25)	1674
F(63)	−1719(49)	379(44)	322(31)	2214
F(64)	−1835(60)	890(49)	718(13)	2028
F(65)	−2454(52)	1245(44)	120(30)	1933
F(66)	−2387(52)	−50(58)	−287(14)	1908
P(7)	3859(21)	6268(24)	4598(9)	983
F(71)	4798(42)	7202(44)	4678(26)	2091
F(72)	4096(55)	5937(51)	4137(15)	2118
F(73)	2919(45)	5338(47)	4506(30)	2487
F(74)	3654(59)	6623(67)	5056(15)	2028
F(75)	4426(58)	5715(59)	4809(19)	1941
F(76)	3304(56)	6827(55)	4387(20)	2201

TABLE 5

AVERAGE METAL–METAL DISTANCES IN *triangulo*-TRIPLATINUM CLUSTERS AND PLATINUM–GOLD CLUSTERS DERIVED FROM THEM

	d(Pt–Pt) (Å)	d(Pt–Au) (Å)
$[Pt_3(\mu\text{-}CO)_3(PCy_3)_3]$	2.655	–
$[Pt_3(\mu\text{-}SO_2)_3(PCy_3)_3]$	2.700	–
$[Pt_3(\mu\text{-}CO)_3(PCy_3)_4]$	2.708	–
$[Pt_3Au(\mu\text{-}CO)_3(PCy_3)_4]^+$	2.696	2.758
$[Pt_3Au(\mu\text{-}CO)_2(\mu\text{-}SO_2)(PCy_3)_4]^+$	2.698	2.758
$[Pt_3Au(\mu\text{-}Cl)(\mu\text{-}SO_2)_2(PCy_3)_3(PAr_3)]^{+a}$	2.864	2.769
$[Pt_3Au_2(\mu\text{-}Cl)(\mu\text{-}SO_2)_2(PCy_3)_3(PAr_3)_2]^{+a}$	2.890	2.785

[a] Ar = *p*-C_6H_4F.

TABLE 6

OVERLAP POPULATIONS CALCULATED BY THE EXTENDED HÜCKEL METHOD FOR SOME *triangulo*-TRIPLATINUM AND PLATINUM–GOLD CLUSTER COMPOUNDS [6]

	Pt–Pt	Pt–Au
$[Pt_3(\mu\text{-}SO_2)_3(PH_3)_3]$	0.186	–
$[Pt_3(\mu\text{-}Cl)(\mu\text{-}SO_2)_2(PH_3)_3]^+$	0.142	–
$[Pt_3Au(\mu\text{-}SO_2)_3(PH_3)_4]^+$	0.161	0.094
$[Pt_3Au(\mu\text{-}Cl)(\mu\text{-}SO_2)_2(PH_3)_4]$	0.113	0.093
$[Pt_3Au_2(\mu\text{-}Cl)(\mu\text{-}SO_2)_2(PH_3)_5]^+$	0.087	0.088

extraction of the residue with benzene a light orange solid was isolated and identified as **1** by IR and $^{31}P\{^1H\}$ NMR spectroscopy. This interesting reaction is similar to the degradation processes observed in gold cluster chemistry, for example:

$$[Au_9(PPh_3)_8]^{3} + I^{-} \xrightarrow{EtOH} [Au_4I_2(PPh_3)_4] \qquad [10]$$

Experimental

Reactions were routinely carried out using standard Schlenk line procedures under an atmosphere of pure, dry N_2 and using dry O_2-free solvents. Microanalyses were carried out by Mr M. Gascoyne and his staff of this laboratory. Infra-red spectra were recorded using a Perkin–Elmer 1710 FT spectrometer. $^{31}P\{^1H\}$ and $^{195}Pt\{^1H\}$ NMR spectra were recorded using a Bruker AM-250 spectrometer operating at 101.26 MHz using TMP (trimethylphosphate) as the external standard, and at 53.55 MHz using Na_2PtCl_6 as the external standard respectively. Tetramethylammonium chloride was used as purchased from BDH Chemicals Ltd.

Preparation of $[Pt_3Au_2(\mu\text{-}Cl)(\mu\text{-}SO_2)_2(PCy_3)_3(P\{p\text{-}C_6H_4F\}_3)_2](PF_6)$ *(2)*

$[Pt_3Au(\mu\text{-}Cl)(\mu\text{-}So_2)_2(PCy_3)_3(P\{p\text{-}C_6H_4F\}_3)]$ [2] (0.20 g, 0.095 mmol) was dissolved in benzene (15 cm^3) and $[AuCl(P\{p\text{-}C_6H_4F\}_3)]$ [11] (0.052 g, 0.095 mmol) was added with stirring. $TlPF_6$ (0.3 g, 0.86 mmol) was added and vigorous stirring continued for 2 h, after which time a yellow-orange solid had formed. The solid was isolated and recrystallised from CH_2Cl_2/hexane to give mustard-yellow crystals of $[Pt_3Au_2(\mu\text{-}Cl)(\mu\text{-}SO_2)_2(PCy_3)_3(P\{p\text{-}C_6H_4F\}_3)_2](PF_6)$ (**2**) in 74% yield. (Found: C, 39.7; H, 4.72. $C_{90}H_{123}AuClF_{12}O_4P_6Pt_3S_2$ calc: C, 39.2; H, 4.4%).

Reaction of **2** *with tetramethylammonium chloride*

$[Pt_3Au_2(\mu\text{-}Cl)(\mu\text{-}SO_2)_2(PCy_3)_3(P\{p\text{-}C_6H_4F\}_3)_2](PF_6)$ (0.1 g) was dissolved in CH_2Cl_2 (10 cm^3) and excess tetramethylammonium chloride added. On stirring for 6 h the colour of the solution had changed from yellow-orange to bright orange. Removal of solvent in vacuo and recrystallisation of the resulting solid from benzene/ethanol gave **1** in 90% yield, identified by $^{31}P\{^1H\}$ NMR spectroscopy.

Crystal structure determination

Mustard yellow crystals of $[Pt_3Au_2(\mu\text{-}Cl)(\mu\text{-}SO_2)_2(PCy_3)_3(P\{p\text{-}C_6H_4F\}_3)_2](PF_6)$ were grown by slow diffusion of hexane into a dichloromethane solution. They were found to be stable in air and to loss of solvent of crystallisation and a single crystal (dimensions $0.20 \times 0.13 \times 0.10$ mm) was mounted in a 0.7 mm Lindemann tube. Details of the data collection are given in Table 2. The structure was solved using Direct Methods (MULTAN) for the metal atoms (Pt and Au) and Fourier Methods for the remaining atoms using atomic scattering factors including anomalous scattering factors from reference [2].

The bridging SO_2 and Cl units in the complex were found to be disordered around the equatorial plane, similar to the situation found in the X-ray analysis of **1**, which crystallised in the space group $P2_1/n$ [2]. The occupancies of the oxygen atoms attached to the equatorial bridging atoms were refined; the refinement converged with occupancies for the oxygens on the sulphur atoms of 0.75, and on

the chlorine atom of 0.50. The isotropic temperature factors of these oxygen atoms were then refined satisfactorily. The large differences in the S–O bond lengths observed in both of these clusters can be attributed to the fact that the disorder between the Cl and S atoms has not been completely resolved.

In addition, the $[PF_6]^-$ counterion was found to be disordered over two crystallographic sites. This was dealt with in a similar manner and the anisotropic temperature factors were found to refine satisfactorily with occupancies of 0.5 in each site.

A table of thermal factors and a list of observed and calculated structure factors are available from the authors.

Acknowledgements

The SERC is thanked for financial support and Johnson-Matthey Ltd for a generous loan of platinum and gold metals.

References

1 C.E. Briant, R.W.M. Wardle and D.M.P. Mingos, J. Organomet. Chem., 267 (1984) C49.
2 D.M.P. Mingos and R.W.M. Wardle, J. Chem. Soc., Dalton Trans., (1986) 73.
3 C.E. Briant, D.I. Gilmour and D.M.P. Mingos, J. Organomet. Chem., 267 (1984) C52; J. Chem. Soc., Dalton Trans., (1986) 835.
4 P. Braunstein, H. Lenner, D. Matt, A. Tiripicchio and M. Tiripicchio-Camellini, Angew. Chem. Int' Ed. Engl., 96 (1984) 307.
5 D.M.P. Mingos and R.W.M. Wardle, unpublished results.
6 D.G. Evans and D.M.P. Mingos, J. Organomet. Chem., 240 (1982) 321; D.I. Gilmour and D.M.P. Mingos, J. Organomet. Chem., 302 (1986) 127.
7 NMR computer simulations were carried out using the Oxford University VAX computer system using a program developed by Prof. R.K. Harris then of the University of East Anglia and adapted for use at Oxford by Dr. A.E. Derome.
8 M.F. Hallam and D.M.P. Mingos, J. Organomet. Chem., 315 (1986) C35.
9 J. Chatt and D.M.P. Mingos, J. Chem. Soc. (A)., (1970) 1243.
10 F.A. Vollenbroek, J.J. Bour, J.M. Trooster and J.W.A. Van der Velden, J. Chem. Soc., Chem. Commun., (1978) 907.
11 F. Bonati and G. Minghetti, Gazz. Chim. Ital., 103 (1973) 373.
12 International Tables for X-ray Crystallography, Kynoch Press, Birmingham, Vol. 4, p. 99.